Mechanosynthesis and Photophysics of Colour-tunable Photoluminescent Group 13 Metal Complexes with Sterically Demanding 3,5-di-*tert*-butyl Substituted Salen and Salophen Ligands

Felix Leon,[†,a] Chenfei Li,[†,a] Javier F. Reynes,[b] Varun K. Sigh,[a] Xiao Lian,[c] How Chee Ong,[a] Gavin Hum,[a] Handong Sun,[c] and Felipe García.*[,b]

[†]Both authors contributed equally

Correspondence to: garciafelipe@uniovi.es

[a] School of Physical and Mathematical Sciences, Division of Chemistry and Biological Chemistry, Nanyang Technological University, 21 Nanyang Link, Singapore.
[b] Departamento de Química Orgánica e Inorgánica, Facultad de Química, Universidad de Oviedo, Julián Claveria 8, Oviedo 33006, Asturias, Spain
[c] School of Physical and Mathematical Sciences, Division of Physics and Applied Physics, Nanyang Technological University, 21 Nanyang Link, Singapore.

Abstract A series of four photoluminescent Al and In complexes were synthesised using an environmentally-benign mechanosynthetic strategy. Both the sterically crowded 3,5-di-*tert*-butyl functionalised salophen, salen ligands and the complexes are synthesised in the solid-state and fully characterised. The photophysics and electrochemistry of these complexes were studied, the results suggested that these novel group 13 complexes can be alternatives of traditional photoluminescent complexes and to avoid the use of organic solvents, helps to reduce the environmental impact of the process and also improves its energy efficiency.

Introduction

Mechanochemistry constitutes an optimal alternative to classical solution-based chemical processes since it allows for chemical transformations to proceed with minimal (or no) solvent involved. In recent years, mechanochemistry has successfully found applications in a wide range of fields (*e.g.*, organometallic chemistry, organo-catalysis, energy materials, API or MOF, among others).[1, 2] Minimising, or avoiding, the use of organic solvents can provide an advantage over conventional solution-based methods by reducing the solvent waste and, thus, eliminating time- and energy-consuming solvent removal steps. In addition, generally, mechanochemical processes do not require external heating for the reactions to proceed. In this context, mechanosynthesis has been growing as a viable alternative to solution-based thermochemistry for the last two decades years.[3,4]

In mechanochemistry, reactions between solids are promoted by the application of mechanical energy, and reactions that often are unfavourable or inaccessible in solutions can be readily performed.[5] The increasing momentum gained by the mechanochemical field is illustrated by its current widespread use in the development of new reaction methodologies,[6,7] synthesis of organometallic complexes,[8,9] main group compounds,[10] metal organic frameworks,[11] alloys,[12] composite materials,[13,14] and co-crystals.[15]. It is worth mentioning that in some mechanochemical reactions, the use of minute amounts solvent is unavoidable, especially in purifications or workup, but this can be avoided in cases of high atomic efficiency or if the by-products can be removed by employing physical separation methods.

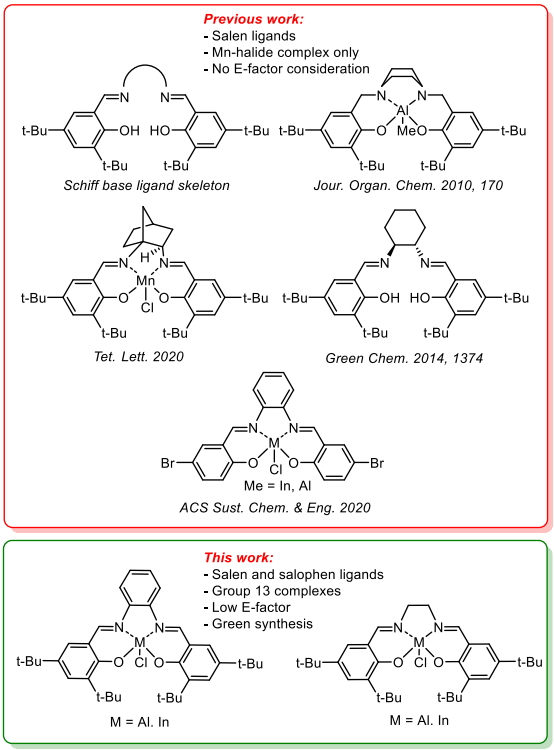

Figure 1. Previously reported salen, salophen and derivative complexes (top). Salen and salophen ligands and the corresponding Al and In complexes described in this work.

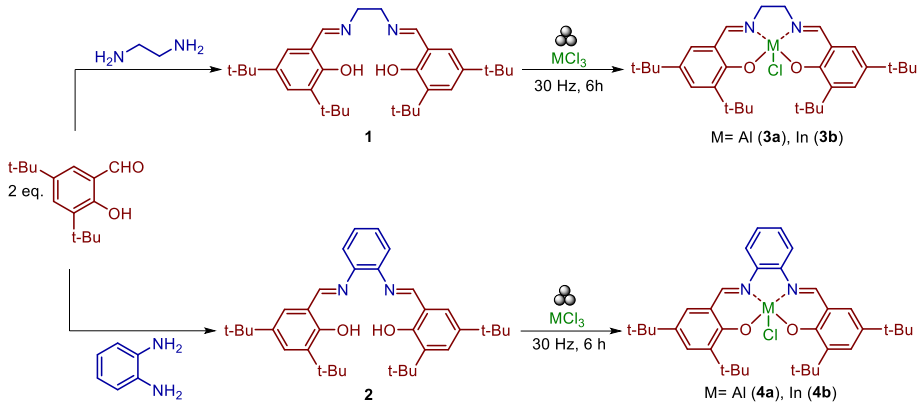

Figure 2. Reaction scheme for ligands **1** and **2** and complexes **3a-4b**.

Photoactive noble metal complexes have been widely applied in organic-light-emitting diodes (OLEDs),[16,17] light-emitting electrochemical cells (LEECs)[18] and photocatalysis.[19,20]. Due to their intrinsic toxicity and scarceness, environmentally benign and low-cost alternatives to heavy metal complexes have long been sought by scientists.[21,22] Currently, photoactive first-row transition metal complexes – obtained *via* traditional solution-based methods - are the mainstream of studies in this field.[23-25]

A less studied alternative to transition metal photoactive species are their main group metal analogues (*i.e.*, such as aluminium, indoum, *etc.*) which are more abundant in the earth's crust (82000 ppm for aluminium *vs* 68 ppm for copper),[26] and less toxic than their noble metal counterparts.

Salen and salophen species constitute an important class of ligands in coordination chemistry due to both their high affinity for various metal ions and their high tuneability through straightforward ligand design.[27,28,29] These ligands have found applications in organic catalysis,[30] polymer synthesis,[31,32,33] stereoselective synthesis,[27,34,35] photoredox catalysis,[36] and also as light-emitting materials in OLEDs,[37,38,39] and sensors.[40,41]

Of particular interest for catalysis are the complexes comprising sterically hindered salen and salophen-based ligand and their metal complexes (**Figure 1**), which have found application in fields such as polymerisation reactions[42] or fluorescence materials.[43,44] These species are often prepared under harsh solvent-based conditions or comprising prolonged refluxing times.[45]

In this regard, James *et al.* recently reported the mechanochemical synthesis of Jacobsen's ligand *via* liquid assisted grinding (LAG) with methanol as a liquid additive, however, the synthesis of its complex was not reported. Moreover, they were also successful in mechanosynthesis of salen complexes with Zn, Cu and Ni under LAG ball-milling conditions and using twin-screw extrusion (TSE).[46] Similarly, Cort and co-workers also reported the mechanosynthesis of salophen ligands and their corresponding Zn, Ni and Pd complexes comprising small methoxy substituents.[47,48,49] More recently, Lamaty *et al.* achieved the mechanosynthesis of sterically demanding manganese complex with 1,2-bicyclo[2.2.2]octane bridge as cytotoxic agents.[50] Within the context of mechanochemically synthesised main group salen and salophen complexes is mainly unexplored. A previously reported example of mechanosynthesis consist of bromo-substituted salen and salophen complexes comprising aluminium and indium metal centres.[51]

In conventional solution synthesis, complexes of the type salen or salophen-MCl (M = main group metal) are commonly prepared using R_2AlCl (R = Me, Et) as the main group metal source. In some cases salen or salophen-MR complexes is formed as side product undesired HCl elimination, and therefore, special reaction conditions such as initial addition of the group 13 reagent to the ligand at lower temperature are required.[52] These considerations, together with our previously success in the synthesis of group 13 salen and salophen complexes,[51] led us to explore main group metal chlorides (MX_3) in solvent-less mechanochemical reaction conditions to allow direct access to main group t-Bu substituted salen and salophen complexes (salen-MCl or salophen-MCl) at room temperature. If successful, developing a mechanochemical approach to sterically bulkier salen and salophen ligands and their main group complexes will contribute to the expansion of new sustainable synthetic routes towards this type of technologically relevant species.

Here, we have investigated the mechanosynthesis of sterically demanding bis(3,5-di-tert-butyl) salen and salophen ligands followed by their complexation with Group 13 metals aluminium (Al) and indium (In). Additionally, we have studied the absorption and emission properties of the newly synthetised complexes as a proof of concept for potential emissive devices application. A complete DFT study has been also carried out to complement and rationalise the observed photophysical properties of the complexes.

Results and Discussions

Synthesis of ligands systems.

In a typical mechano synthesis of bis(3,5-di-tert-butyl) salen (**1**) and bis(3,5-di-tert-butyl)-salophen (**2**) ligand, 3,5-di-tert-butyl salicyaldehyde (2 eq) and either ethylene diamine (1 eq) or 1,2-phenylene diamine (1 eq) was grounded together in a 10 mL ball milling jar with a 8 mm diameter steel ball, respectively (**Figure 2**). The reaction progress was monitored by ^{1}H NMR by measuring the ratio of aldehyde peak at 9.85 ppm in starting material with respect the imine peak at 8.44 ppm in the case of **1** and 8.73 ppm in the case of **2** in $CDCl_3$. The mechanosynthesis of **1** proceeded smoothly and achieved full conversion in two hours with 93% isolated yield. The ^{1}H NMR exhibited six peaks which were assigned to OH protons (13.70 ppm), imine CH=N protons (8.44 ppm), aromatic protons (7.43 and 7.12 ppm), ethylene protons (3.95 ppm) and t-Bu protons (1.50-1.34 ppm). ^{13}C NMR spectrum also exhibited C=N signals at 167.6 ppm as well as disappearance of aldehyde carbon signal of the starting material (197.3 ppm). These results were encouraging especially because

the synthesis didn't require any solvent and heating as opposed to conventional solution methods. Encouraged by these results, we attempted the mechanosynthesis of **2** under similar reaction conditions as used in salen ligand synthesis. However, the salophen derivative synthesis showed very small conversion after two hours of milling time and a mixture of diimine and monoamine was observed with monoamine being the major product. Slow reaction progress in mechanosynthesis of aryl backboned ligands have been observed before by James and co-workers with salen ligand synthesis involving bulkier bis(3,5-di-tert-butyl) groups.

Table 1. Mechanochemical conditions for the synthesis of ligands 1 and 2 and complexes 3a-4b with calculated conversion and yields. Reactions required LAG for complete conversion [46]

Compound	Freq (Hz)	T (h)	Conversion (%)	Yield (%)
1	30	2	100	93
2	30	2	100	90
3a	30	6	100	85
3b	30	6	100	88
4a	30	6	100	79
4b	30	6	100	70

With the aim to optimise the reaction, we attempted LAG with a variety of solvents. While LAG does reduce the solvent-free nature of the synthesis, the amount of solvent used (1 molar equivalent) are much less than the amount of solvent that would be needed otherwise in conventional solution synthesis. For LAG we tested the synthesis in the presence of acetone, tetrahydrofuran and methanol. After 8 h, the reaction in acetone and tetrahydrofuran resulted in 52% and 56% yield of diimine product, respectively, with a mixture of monoamine. While reaction with methanol gave 40% yield of diimine after 4 h. In an attempt to improve the conversion, the reaction time was extended to 8 h, yielding a rather low conversion of 60% Other proposed methods of speeding up mechanochemical reactions in the literature suggested that the rate of conversion is proportional to the energy imparted by the associated impact. [53] We then decided to study the effect of changing the ball and jar material from the standard steel to denser materials like tungsten carbide, which produces more kinetic energy due to its higher density (15.6 g/cm^3 compared to steel 7.9 g/cm^3). However, attempts at synthesis of **2** using a tungsten carbide ball of 8 mm in tungsten carbide jar led to a complex mixture of products. As to why salophen ligand did not undergo to full conversion, we hypothesised the primary barrier was kinetic obstacles due to the weaker nucleophilicity of 1,2-phenylene diamine compared to ethylene diamine and an electron rich character of 3,5-di-tert-butyl salicyaldehyde. Therefore, we thought using an acid in a catalytic amount could help activate the carbonyl carbon thus reducing the activation energy. To our delight, with acetic acid as catalyst the reaction was completed with 100% conversion and 90% yield in 3 h using a steel ball and steel jar as the reaction vessel. The full conversion was confirmed by ^{1}H NMR as the peaks due to mono-substituted imine and the signals of bis(3,5-di-tert-butyl) benzaldehyde disappearance.

Synthesis of metal complexes

Following these results, we next studied the mechanochemical complexation of **1** and **2** with aluminium and indium. In the initial trials $AlCl_3$ and $InCl_3$ were added directly to the milling jars with salenH_2 or salophenH_2 ligands, however, milling under these conditions for four hours resulted in incomplete conversion and partial hydrolysis of the imine bond, presumably due to the formation of HCl as well as the potential presence of traces of water formed as by-product in the initial ligand reaction step. Therefore, oven dried anhydrous magnesium sulphate was used as dehydrating agent along with reaction mixture and the complexation reaction were done in inert atmosphere using air-tight milling jars for six hours. This approach resulted in complete consumption of the ligand as marked by the disappearance of the phenolic group ligand NMR signal, as well as changes in the chemical shifts of other resonances, particularly the imine protons, indicating full conversion in both cases (**Table 1**).

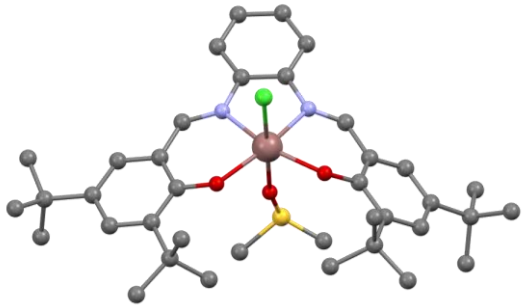

Figure 3. X-Ray structure of **4b**. Hydrogen atoms are omitted for clarity

In the case of Bis(3,5-di-tert-butyl) salen-M(Cl) complexes (M= Al (**3a**) and In (**3b**)) were prepared by reacting one equivalent of **2** with 1.5 equivalents of the corresponding metal trihalide and 12 equivalent of magnesium sulphate. The yield was determined by ^{1}H NMR analysis, the imine peak at 8.44 ppm was shifted to 8.43 ppm (Al) and 8.75 ppm (In), respectively, with the disappearance of the respective phenolic peaks.

In an analogous manner, complexes bis(3,5-di-tert-butyl) salophen-M(Cl) complexes (M= Al and In, **4a** and **4b**, respectively) were obtained by reacting one equivalent of **2** was reacted with 1.5 equivalent of the metal source and 13 equivalent of magnesium sulphate. During the formation of the complex, ^{1}H NMR spectrum showed that the imine peak in the free ligand at 8.73 ppm was shifted to 9.03 and 8.85 ppm (for Al and In) together with the disappearance of phenolic ligand signal.

The newly synthetised compounds were fully characterised using all the relevant spectroscopic techniques (^{1}H and ^{13}C{^{1}H} NMR, FT-IR, UV-VIS and TOF-MS). In addition, attempts to obtain crystals suitable for SCXR (single crystal X-ray) analysis were carried out. However, the complexes shown poor to none solubility in mostly of organic solvents with the exception of DMSO and DMF. Unfortunately, only single crystals of **4b** were obtained. Yellow crystals suitable for X-ray diffraction studies were obtained by slow cooling of a saturated solution of **4b** in boiling DMSO (**Figure 3**). The SCXR studies of **4b** show two chemically equivalent – but crystallographically distinct – molecules in the unit cell. Complex **4b** displays an octahedral geometry with the two-imine nitrogen and the two phenolic oxygens occupying the equatorial plane, with an average N-In and O-In distances of 2.208 and 2.071 Å, respectively. The chlorine atom is located in one of the axial positions with a Cl-In distance of 2.491 Å. The remaining axial position is occupied by a molecule of DMSO, coordinated through the oxygen atom, with a O-In distance of 2.315 Å.

Notably, while the backbone phenyl group is coplanar with respect the equatorial plane defined by the ligand N and O atoms, the flanking t-Bu substituted aryl groups are bent out of that plane towards the coordinated DMSO. Thus, the C4-In-C4' angle (C4 and C4' = *p*-C to the coordinated oxygen) is 129.16°. This deviation from the coplanar geometry is presumably due to the sterically hindered accommodation of the In atom. Indeed, in structurally related salen complexes with less bulky Zn metal centre (empirical radii 135 pm vs 155 pm for In), the same angle presents a much more coplanar arrangement (C4-Zn-C4´ 157.35°).[47]

DFT and Photophysics studies

In order to obtain more structural information of complexes **3a-4b** a DFT optimisation of all the structures was carried out at the B3W91-D3/SSD/SMD (solvent = DMSO) level of theory, although the coordinated DMSO molecule was omitted in order to simplify the calculations. Our theoretical studies started by comparing the optimised structure of **4b** with the experimental X-Ray structure (**Figure 4**). The computed N-In distances in **4b** are 2.18 and 2.19 Å, while the O-In distances are 2.02 and 2.03 Å, nicely matching the experimental data obtained. The computed In-Cl distance of 2.38 Å is found to be slightly shorter than respect the experimental one, presumably due to the lack of coordinated DMSO in the computed structure with the consequent absent of *trans* influence. Finally, the out of plane bending of the flanking aryl groups is also observed in the computed structure, although with a smaller C4-O-O-C4' dihedral out of plane deviation of 162.2°. Interestingly, the computed structure of **3a** also displays a bent conformation of the flanking aryl groups (C4-O-O-C4' dihedral out of plane deviation of 144.3°). The N-Al (1.98 and 1.99 Å) and O-Al distances (1.82 and 1.81 Å) are considerably shortened with respect **4b**, as well as the Al-Cl distance which is found to be 2.24 Å. In the case of the Al-salophen derivative **3b** the flaking aryl groups out of plane deviation (156.7°) is close to the one found in In analogous **4b** although with a considerably shorter In-Cl distance of 2.23, very similar to the Al-Cl distance observed in **3a**. The N-Al distances in **3b** are very close to the ones found in **3a** (1.99 and 2.01 Å), A similar observation is made of the O-Al distances (1.82 and 1.81 Å). Finally, The In-salen complex **4a** shows an out of plane dihedral deviation of the flanking aryl groups of 166.87°, an In-Cl distance close to the one found in the In-salophen derivative **4b** of 2.39 Å, as well a comparable N-In (2.17 and 2.17 Å) and O-In distances (2.04 and 2.03 Å).

The computed structures were then used to carry out a TD-DFT study of the complexes. Firstly, the UV-Vis spectra for **3a**-**4b** were simulated, and to our delight they nicely matched the experimentally obtained ones. The absorption spectra of salen and salophen complexes measured in DMSO are shown in **Figure 5**, the transition oscillator strengths predicted by TD-DFT are shown as bars within the same figure. MO diagrams with Mulliken population analysis can be found in **Figure S34.** Regarding the two salen-based complexes, a broad and unstructured absorption band in UVA (320-400 nm) region was found in both absorption spectrum, while the absorption peak for this band of **3a** is higher in energy than that of **3b** (360 nm for **3a**, and 331 nm for **3b**). The zero-zero transition energy ($E_{0,0}$) calculated from the intersection point of normalised UV and PL spectra is 3.804 and 3.836 eV for **3a** and **3b**, respectively.[54] According to TD-DFT calculation, transitions from HOMO-1 to LUMO and HOMO to LOMO+1 had a major contribution to the lower energy band for both complexes. Both transitions have a mixture of ligand centred π-π* character (mainly on phenyl rings) and charge transfer character (from phenyl ring π orbital/ oxygen p orbital to the Schiff base bridge). The energies of these transitions are similar (371 & 360 nm for **3a**, 367 & 331 nm for **3b**). At higher energy region, **3a** shows another absorption band at 280 nm while the corresponding absorption band of **3b** is 270 nm, slightly higher energy than DMSO UV cut-off. A highly allowed transition with a mixture of ligand centred π-π* character (mainly on phenyl rings) and charge transfer character (from oxygen p orbital to the Schiff base bridge) was found for both complexes (λ = 283 nm, *f* = 0.2223 for **3a**, λ = 279 nm, *f* = 0.3668 for **3b**). Compared to structurally similar Salen-Al complexes (**Figure 7**) reported by Do *et al*., **3a** and **3b** showed similar UV-Vis absorption spectra while the absorption bands of **3a** and **3b** have slightly higher energy. More recently, Che *et al*.[55] reported a series of phosphorescent dioxo Tungsten (VI) salen complexes, comparing to them, **3a** and **3b** exhibited larger band gap and higher absorptivity due to a larger HOMO/LUMO overlap.

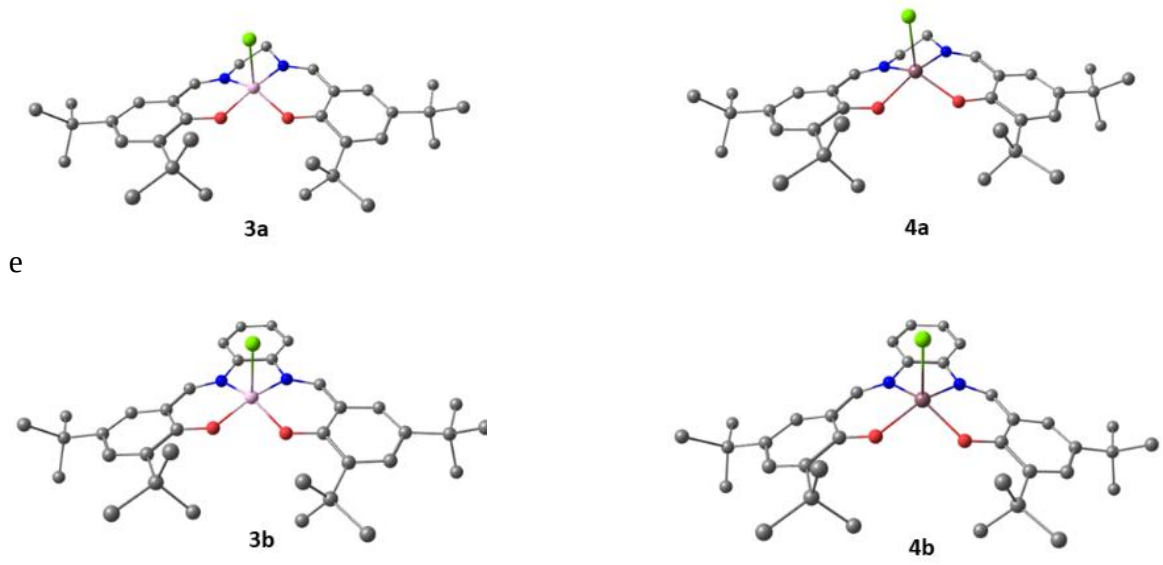

e

Figure 4. DFT computed structures of **3a-4b**

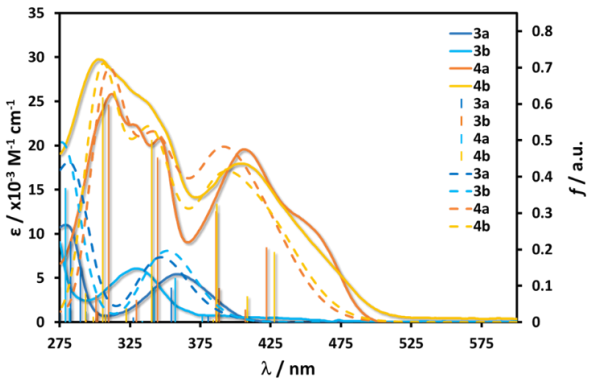

Complex	λ/nm (ε / x10^{-3}M^{-1}cm^{-1})	λ/nm (No. of state)	f^a	Character^b
3a	280 (10.99)	283 (6)	0.2223	CTO->N bridge, LCPh
	360 (5.43)	341 (3)	0.0989	CTPh,O->N bridge, LCPh
		354 (2)	0.0948	CTPh,O->N bridge, LCPh
3b	-	279 (7)	0.3688	CTO->N bridge, LCPh
	331 (6.07)	342 (3)	0.0959	CTPh,O->N bridge, LCPh
		357 (2)	0.1220	CTPh,O->N bridge, LCPh
4a	314 (25.57)	310 (7)	0.5981	LCPh, N bridge
	330 (22.23)^c	330 (6)	0.0611	LCPh, N bridge
	343 (20.47)	345 (5)	0.4526	LCPh, N bridge
	409 (19.43)	386 (4)	0.3053	CTPh,O->N bridge, LCPh
	448 (10.24)^c	422 (1)	0.2065	CTPh,O->N bridge, LCPh
4b	303 (29.77)	306 (8)	0.6176	LCPh, N bridge
	338 (24.76)^c	340 (5)	0.5016	LCPh, N bridge
	407 (17.91)	387 (3)	0.3258	CTPh,O->N bridge, LCPh
		428 (1)	0.1931	CTPh,O->N bridge, LCPh

Figure 5. Experimental (solid lines) and computed (dashed lines) of **3a-4b** and table summarising the energy of major transitions calculated by TD-DFT (a) oscillator strength calculated by TD-DFT (b3pw91-D3/SDD-DMSO); (b) Mulliken population analysed by Chemissian; (c) shoulder peak

On the other hand, intensive absorption from 280 nm to 500 nm was found with two major humps for the two salophen complexes (**4a** and **4b)**. At lower energy region (375 to 475 nm), both salophen complexes absorb intensively while **4a** complex showed a shoulder hump at 448 nm and a peak at 409 nm which is close to the absorption peak of **4b** (407 nm). Compared to Salen analogues, having conjugated Phenyl linkage lead to a smaller zero-zero transition energy ($E_{0,0}$ = 3.486 and 3.445 eV for **4a** and **4b**, respectively). According to TD-DFT calculation, transitions from HOMO-1 to LUMO and HOMO to LOMO+1 had a major contribution to the lower energy band for both complexes. Both transitions have a mixture of ligand centred π-π* character (mainly on phenyl rings) and intraligand charge transfer character (from phenyl ring π orbital/ oxygen p orbital to the Schiff base bridge). The energies of these transitions are similar (371 & 360 nm for **3a**, 367 & 331 for **3b**). Compared to two Salen complexes, due to the conjugated phenyl linkage, π-bonding orbitals of Schiff base bridge contributed more to HOMO for both Salophen complexes.

At higher energy region, both complexes show structured absorption band at 305 nm while the corresponding absorption band of **4a** is structured with three humps (288, 315, 343 nm), while **4b** has a peak (303 nm) and a shoulder peak (338 nm) region. Several highly allowed transitions with a mixture of ligand centred π-π* character (mainly on phenyl rings) and intraligand charge transfer character (from oxygen p orbital to the Schiff base

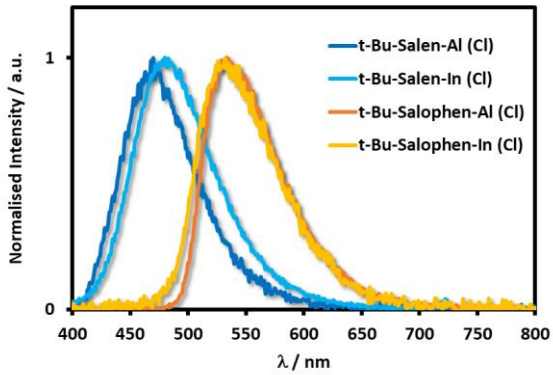

Complex	λ / nm^a	Φ_{PL} / %^{a}	τ_{PL} / ns^b	k_r / ns^{-1c}	k_{nr} / ns^{-1c}	FWHM / cm^{-1}	CIE$_{1931}$
3a	470	7.6(22.5)	0.70	0.11	1.32	3175	0.15,0.20
3b	480	3.7(14.0)	3.44	0.01	0.28	3398	0.17,0.29
4a	532	2.2(2.1)	0.24	0.09	4.08	2453	0.36,0.60
4b	533	2.5(0.4)	0.21	0.12	4.64	2629	0.34,0.59

Figure 6. Emission spectra of salen and salophen complexes in DMSO, excited at 360 nm and summarised data of the emission. (a) excited at 360 nm; (b) excited at 400 nm; (c) radiative and non-radiative rate constants were calculated using equation $k_r = \frac{\Phi_{PL}}{\tau}$; $k_{nr} = \frac{1-\Phi_{PL}}{\tau}$

bridge) was found for both complexes (λ = 310 and 345 nm, *f* = 0.5981 and 0.4526 for **4a**, λ = 306 and 340 nm, *f* = 0.6176 and 0.5016 for **4b**) and the predicted oscillator strengths were found consistent with experimental results.

All four complexes were found emissive, the photoluminescent properties of salen and salophen complexes were studied in DMSO. The PL spectra and the photophysical properties are summarised in **Figure 6**.[55]

Bright blue emissive **3a** (λ_{max} = 470 nm) was found the most emissive amongst the four with a photoluminescent quantum yield (Φ_{PL}) of 7.6%. The CIE1931 coordinate of **3a** emission is (0.15, 0.20, **Figure S28**) while the Full width at half maximum (FWHM) is 3175 cm^{-1}. Compared to previously studied blue emitters based on Salen-Al complexes, the λ_{max} of **3a** blue shifted to ~440 cm^{-1}.[56] In contrast to what we observed in UV-Vis spectra, where **3b** showed higher energy absorption than that of **3a**, the emission energy of **3b** is 443 cm^{-1} smaller than **3a** with a slightly broader emission band (FWHM = 3398 cm^{-1}), the emission colour of **3b** in DMSO is azure-blue with a CIE1931 coordinate of (0.17, 0.29). Alongside the red-shift of emission spectrum, the Φ_{PL} of **3b** (3.7%) is also lower compared to **3a**.

Both the salophen complexes **4a** and **4b** showed emerald emission with λ_{max} at 532 and 533 nm, respectively. Although the Φ_{PL} for both salophen complexes were low (2.2% for **4a** and 2.5% for **4b**), the emission bands were narrower compared to salen complexes. **3a** exhibited the smallest FWHM of 2453 cm^{-1} amongst the four complexes while the FWHM of **3b** was only 176 cm^{-1} larger.

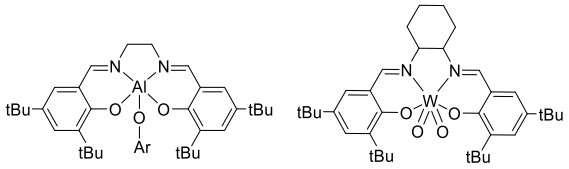

Figure 7. Representative examples of emissive salen metal complexes.

The S_1 state of all four complexes are attributed mainly to the HOMO to LUMO transition which in all cases has a mixture of intraligand charge transfer (from oxygen p-orbital and Phenyl π-orbital to Schiff base bridge π* orbital) character and localised π-π* character. Hence, all four complexes exhibited unstructured emission bands.

The photoluminescent lifetime was studied in DMSO solution, using a femtosecond amplified laser excitation source (400 nm). Amongst the four complexes, **3a**, **4a** and **4b** complexes showed photoluminescence lifetime shorter than 1 ns (0.70, 0.24 and 0.21 ns, respectively). The short-excited state lifetimes of two salophen complexes were in part due to the larger non-radiative decay rate constant which also lead to a smaller Φ_{PL} compared to salen complexes. While having the largest Φ_{PL} within the four, **3a** complex showed way shorter excited state lifetime than **3b** (τ = 3.44 ns). This was due to the smaller radiative decay rate constant found for **3b** (k_r = 0.01 ns^{-1}) which is the smallest one amongst the four, while the other three complexes have similar k_r around 0.1 ns^{-1}. According to our TD-DFT studies, the S_1 state of **3b** has the most CT character which is consistent with the fact that **3b** complex has the largest Stokes shift among the four (9608 cm^{-1}).

Assessment of Environmental Impact

Finally, we carried out a detailed assessment of the environmental impact of mechanosynthesis of salen and salophen complexes with Indium and Aluminium and compared it with previously reported environmental assessments for the similar type of complexes.[51]

To determine the environmental impact, green chemistry metrics (GCM)[51] were calculated. Firstly, E-factor was estimated. E-factor constitutes a GCM to address the greenness of a synthesis method.[57,58,59]. Then, process mass intensity (PMI) and reaction mass efficiency (RME) for both mechanochemical and solution-based synthetic routes were calculated. **Table 2** summarized these metrics. Detailed calculations can be found in the SI (section B). Under mechanochemical conditions, low E-factor have been observed, ranging from 0.4 to 4.03 (**Table 2**). It is observed the under conventional solution-based synthetic routes, the E-factors are higher ranging from 2.05 to 5.19.

Then, the PMI was determined in order to see how well it aligns with the E-factor (see **SI**). The PMI is defined by the ratio between the quantity of raw material used along the process and the amount of product obtained,[51] making it an ideal metric to compare mechanosynthesis and conventional solution-based synthesis. **Table 2** shows that mechanochemical PMI values are much smaller (1.02 to 1.66) than those obtained by convention-solution based method (3.17 to 28.9), which further demonstrates the reduced environmental footprint of mechanosynthesis compared to traditional solution-based methods.

Finally, the reaction mass efficiency was estimated to understand the environmental impact of each compound in the reaction comparing the two synthetic routes. Results (**Table 2**) shows that mechanochemistry routes have higher RME that its counterpart prepared by solution-based method (*i.e.*, 60 % to 49 % for complex **4b**). These results further support that the mechanochemical route is much better environmentally than the conventional one.

Since salen and salophen complexes have similar synthetic routes, the results obtained in this work for small-scale reactions can be extrapolated to upper-scale based on the literature,[51] where it has been demonstrated that at different scales, up to 120 grams of reagent, a full conversion with 95% yield was achieved as analysed by ^{1}H NMR spectroscopy.

Table 2. Green metrics comparison of mechanosynthesis and conventional solution-based synthesis of ligands 1 and 2 and complexes **3a to 4b.**

Compound	E-factor	PMI	RME (%)
Mechanochemistry method			
1	0.40	1.02	98
2	0.31	1.06	95
3a	3.02	1.13	89
3b	3.93	1.55	64
4a	3.83	1.42	70
4b	4.03	1.66	60
Conventional solution-based method*			
1	2.05	3.17	82
2	2.29	3.30	75
3a	4.76	39.7	53
3b	5.03	28.8	47
4a	4.92	28.7	43
4b	5.19	28.9	49

*Solution-based synthesis

Energy efficiency costs

Although the environmental performance of the process is a key parameter, other aspects such as cost, and energy efficiency must also be considered to design the most suitable synthetic pathway for the any given target, specially in the case of technologically and catalytically relevant species – such as salen and salophen complexes. For this purpose, the energy efficiency and cost disparity between the mechanochemical and solution-based approaches has been assessed.

The energy consumption was calculated by considering maximum power consumption during the milling process and negligible when idle. As for the solution-based methodology, we considered the hot plate to be at maximum power while heating and meaningless power when only stirring, which is in line with previous energy consumption reports.[51]

All ligands and complexes (**1 to 4b**) have been synthesized by both mechanochemistry and conventional methods solution-based at small scale (0.1 g).[60] Despite literature report indicating that the solution-based methods requiring 17 hours to obtain the ligands (**1,2**), we observed that *ca.* 12 hours is sufficient for their synthesis. Therefore, refluxing for 12 hours has been used throughout our study to provide a more accurate assessment of energy consumption (**SI, section B-2**).

The energy consumption and % energy saved projections were estimated at the low scale reported here as well as predicted using upscaled synthesis of salen and salophen complexes previously reported in the literature (**Table 3**) (see **SI, section B-2**).[51]

Our energy consumption calculations show mechanochemical methods requiring less energy in all cases. For the complex upscaled synthesis (*i.e.*, 120 g) of complex, the mechanochemical process projected consumption is ~12.8 kW·h, which translated to 384 $MJ \cdot kg^{-1}$ of product, while the energy consumption projected for solution-based synthesis required ~19.2 kW·h, which is equivalent to 512 MJ·kg−1 (107 $kW \cdot h \cdot kg^{-1}$). The energy consumption for the synthesis of complexes 3a to 4b at different scales is summarized in Table S1 (SI).

It is worth highlighting despite upscaling reduces the energy saved (**Table 3**) between both methods significantly. This is mainly due to the fact that based on energy consumption results, 120 g of product could be produced with similar energy cost provided identical reaction times are used.[51] However, we would expect that continuous processes, such as twin-extrusion, and other mechanochemical intensification approaches would provide

better energy saving that high frequency vibratory mills [61,62]as it has been already demonstrated for active pharmaceutical ingredients (APIs) produced mechanochemically.

Finally, we estimated the electricity costs in order to determine how energy consumption translated into industrial production costs. For this purpose, an average price of electricity to household and non-household medium size consumer throughout the European Union (including UK) as well as the average cost was estimated; see section **Table 3** and **SI**.

As expected, the electricity costs using mechanochemistry method are substantially lower than the one obtained by conventional solution-based method (*i.e.*, 1167.3 €·kg^{-1} *vs* 18681.0 €·kg^{-1}). Although the average cost per kg obtained in this article have been directly calculated for a small scale (0.1 g), for consistency and direct comparison with the literature,[51] upscaling projections shows that costs per kg dramatically decreases as the scale increases in all cases. Our projections indicate that mechanochemistry will offer a cost reduction at larger scales – specially with twin-extrusion, and other mechanochemical intensification approaches – making it a promising for industrial scale synthesis of OLEDs at different scales.[17,22]

Table 3. Energy consumption and cost comparison to non-household, medium size consumers in euro for the synthesis of complexes **3a** to **4b** at different scales*

Scale (g)	Energy Consumption*** (MJ.kg^{-1})	Approx. Electricity cost (€.kg^{-1})**	Energy difference (%)
Mechanochemistry method			
0.1	43200	1167.3	93.8
1.0 [P)]	4320	116.7	93.8
30.0[(P)]	1200	32.4	47.9
60.0[(P)]	600	16.2	47.9
120.0[(P)]	384	10.4	25
Conventional solution-based method* **			
0.1	691200	18681.0	
1.0[(P)]	69120	1868.1	
30.0[(P)]	2304	62.3	
60.0[(P)]	1152	31.1	
120.0[(P)]	512	13.8	

***For ligands 1 and 2 and medium size household consumers check SI (Table S3). For formula check SI (section B-2).**
****Calculated based on average values of Table S4 (SI)**
*****Calculated based on Energy usage calculations (SI – B-2)**
[(P)] Larger-scale projections based on literature values.[51]

Nevertheless, as our calculations are only based on energy consumption, costs related with the use of solvents (*i.e.*, transportation, recycling or disposal) have not been considered. Therefore, it can be predicted that the advantage of mechanochemistry will remain even at larger scales.

Acknowledgements

F.G. would like to thank A*STAR AME IRG (A1783c0003 and A2083c0050), NTU for a start-up grant (M4080552) and MOE Tier 1 grants (RG 11/15 and RG 113/16) . F. G. also thanks the support of Fundación para el Fomento en Asturias de la Investigación Científica Aplicada y la Tecnología (FICYT) through the Margarita Salas Senior Program (AYUD/2021/59709).

REFERENCES

1. S. L. James and T. Frišcic, *Chem. Soc. Rev*, 2013, **42**, 7494-7496.
2. K. T. Yeung, W. P. To, C. Sun, G. Cheng, C. Ma, G. S. M. Tong, C. Yang and C. M. J. A. C. Che, 2017, **129**, 139-143.
3. J.-L. Do and T. J. A. c. s. Friščić, 2017, **3**, 13-19.
4. T. Friščić, C. Mottillo and H. M. J. A. C. Titi, 2020, **132**, 1030-1041.
5. L. J. C. S. R. Takacs, 2013, **42**, 7649-7659.
6. G.-W. J. C. S. R. Wang, 2013, **42**, 7668-7700.
7. T. K. Achar, A. Bose and P. Mal, *Beils. J. Org. Chem.*, 2017, **13**, 1907-1931.
8. K. Kubota, R. Takahashi and H. Ito, *Chem. Science*, 2019, **10**, 5837-5842.
9. R. Zaky and A. Fekri, *Applied Organom. Chem.*, 2019, **33**, 1-16.
10. A. A. Gečiauskaitė and F. J. García, *Beils. J. Org. Chem.*, 2017, **13**, 2068-2077.
11. D. Chen, J. Zhao, P. Zhang and S. Dai, *Polyhedron*, 2019, **162**, 59-64.
12. V. K. Portnoi, V. A. Leonov, S. E. Filippova, A. I. Logacheva, A. G. Beresnev and I. M. Razumovskii, *Inorg. Mater.*, 2016, **52**, 895-901.
13. B. Szczesniak, S. Borysiuk, J. Choma and M. Jaroniec, *Mater. Horiz.*, 2020, **7**, 1457-1473.
14. T. F. Grigorieva, A. P. Barinova and N. Z. Lyakhov, *J. Nanopart. Res.*, 2003, **5**, 439-453.
15. D. Braga, L. Maini and F. Grepioni, *Chem. Soc. Rev*, 2013, **42**, 7638-7648.
16. A. F. Henwood and E. Zysman-Colman, *Chem. Commun.*, 2017, **53**, 807-826.
17. A. Zampetti, A. Minotto and F. Cacialli, *Adv. Func. Mat.*, 2019, **29**, 1-22.
18. A. F. Henwood and E. Zysman-Colman, *Top. Curr. Chem.*, 2016, **374**, 1-41.
19. C. K. Prier, D. A. Rankic and D. W. C. MacMillan, *Chem. Soc. Rev*, 2013, **113**, 5322-5363.
20. M. Parasram and V. Gevorgyan, *Chem. Soc. Rev*, 2017, **46**, 6227-6240.
21. B. M. Hockin, C. Li, N. Robertson and E. Zysman-Colman, *Cat. Sc.Tech,*, 2019, **9**, 889-915.
22. C. Bizzarri, E. Spuling, D. M. Knoll, D. Volz and S. Bräse, *Coord. Chem. Rev.*, 2018, **373**, 49-82.
23. F. Glaser and O. S. Wenger, *Coord. Chem. Rev.*, 2020, **405**, 213129-213129.
24. C. B. Larsen and O. S. Wenger, *Chem. Eur. J.*, 2018, **24**, 2039-2058.
25. O. S. Wenger, *J. Am. Chem. Soc.*, 2018, **140**, 13522-13533.
26. A. A. Yaroshevsky, *Geochem. Inter.*, 2006, **44**, 48-55.
27. P. Pfeiffer, E. Breith, E. Lübbe and T. Tsumaki, *Justus Liebigs Ann. Chem.*, 1933, **503**, 84-130.
28. P. G. Cozzi, *Chem. Soc. Rev*, 2004, **33**, 410-421.
29. C. Baleizão and H. Garcia, *Chem. Soc. Rev*, 2006, **106**, 3987-4043.
30. J. A. Castro-Osma, K. J. Lamb and M. North, *ACS Catal.*, 2016, **6**, 5012-5025.
31. H. Li and Y. Niu, *Polym. J.*, 2011, **43**, 121-125.
32. M. Cozzolino, V. Leo, C. Tedesco, M. Mazzeo and M. Lamberti, *Dalt. Trans.*, 2018, **47**, 13229-13238.
33. M. Zhang, J. Xie and C. Zhu, *Nat. Comm.*, 2018, **9**, 1-10.
34. A. Gualandi, F. Calogero, S. Potenti and P. G. Cozzi, *Molec.*, 2019, **24**.
35. K. Matsumoto, B. Saito and T. Katsuki, *Chem. Commun.*, 2007, DOI: 10.1039/b701431g, 3619-3627.
36. A. Gualandi, M. Marchini, L. Mengozzi, H. T. Kidanu, A. Franc, P. Ceroni and P. G. Cozzi, *Eur. J. Org. Chem.*, 2020, **2020**, 1486-1490.
37. K. Y. Hwang, H. Kim, Y. S. Lee, M. H. Lee and Y. Do, *Chem. Eur. J.*, 2009, **15**, 6478-6487.
38. S. H. Lee, N. Shin, S. W. Kwak, K. Hyun, W. H. Woo, J. H. Lee, H. Hwang, M. Kim, J. Lee, Y. Kim, K. M. Lee and M. H. Park, *Inorg. Chem.*, 2017, **56**, 2621-2626.
39. Y. Chen, X. Li, N. Li, Y. Quan, Y. Cheng and Y. Tang, *Mater. Chem. Front.*, 2019, **3**, 867-873.
40. J. Cheng, X. Ma, Y. Zhang, J. Liu, X. Zhou and H. Xiang, *Inorg. Chem.*, 2014, **53**, 3210-3219.
41. V. Sathish, A. Ramdass, M. Velayudham, K. L. Lu, P. Thanasekaran and S. Rajagopal, *Dalt. Trans.*, 2017, **46**.
42. Y. Liang, R.-L. Duan, C.-Y. Hu, L.-L. Li, X. Pang, W.-X. Zhang and X.-S. Chen, *Chin. J. Polym. Sci.*, 2018, **36**, 185-189.
43. J. Cheng, K. Wei, X. Ma, X. Zhou and H. Xiang, *Chin. J. Polym. Sci.*, 2013, **117**, 16552-16563.

44. X. Zhang, J. Shi, J. Song, M. Wang, X. Xu, L. Qu, X. Zhou and H. Xiang, *ACS Om.*, 2018, **3**, 8992-9002.
45. N. C. Johnstone, E. S. Aazam, P. B. Hitchcock and J. R. Fulton, *J. Organom. Chem.*, 2010, **695**, 170-176.
46. M. Ferguson, N. Giri, X. Huang, D. Apperley and S. L. James, *Green Chem.*, 2014, **16**, 1374-1382.
47. C. Zn, P. Complexes, L. Leoni, A. Carletta, L. Fusaro, J. Dubois, N. A. Tumanov, C. Aprile, J. Wouters and A. D. Cort, *Molec.*, 2019, **24**, 1-10.
48. D. Crawford, J. Casaban, R. Haydon, N. Giri, T. McNally and S. L. James, *Chem. Science*, 2015, **6**, 1645-1649.
49. D. E. Crawford, C. K. Miskimmin, J. Cahir and S. L. James, *Chem. Commun.*, 2017, **53**, 13067-13070.
50. P. Milbeo, F. Quintin, L. Moulat, C. Didierjean, J. Martinez, X. Bantreil, M. Calmès and F. Lamaty, *Chem. Rev.*, 2020, **10.26434/c**.
51. F. Garcia, H. C. Ong and V. K. Singh, *Inorg. Chem. Commun.*, 2020.
52. D. Rutherford and D. A. Atwood, *Organom.*, 1996, **15**, 4417-4422.
53. D. A. Fulmer, W. C. Shearouse, S. T. Medonza and J. MacK, *Green Chem.*, 2009, **11**, 1821-1825.
54. S. Chibani, B. Le Guennic, A. Charaf-Eddin, A. D. Laurent and D. Jacquemin, *J. Chem. Sc.*, 2013, **4**, 1950-1963.
55. V. V. N. Ravi Kishore, K. L. Narasimhan and N. Periasamy, *Chem. Phys. Lett.*, 2003, **5**, 1386-1391.
56. G. Cheng, C. Ma, G. So, M. Tong, K.-t. Yeung, W.-p. To, C. Sun, G. Cheng, C. Ma and G. So, *Angew. Chem. Int. Ed.*, 2017, 133-137.
57. R. A. Sheldon, *Green Chem.*, 2017, **19**, 18-43.
58. C. Petrucci, G. Strappaveccia, F. Giacalone, M. Gruttadauria, F. Pizzo and L. Vaccaro, *ACS Sust. Chem. Eng.*, 2014, **2**, 2813-2819.
59. R. A. Sheldon, *ACS Sust. Chem. Eng.*, 2018, **6**, 32-48.
60. R. A. Kemp and T. J. Boyle, *Google Patents*, 2020.
61. P. Sharma, C. Vetter, E. Ponnusamy and E. Colacino, *ACS Sust. Chem. Eng.*, 2022, **10**, 5110-5116.
62. O. Galant, G. Cerfeda, A. S. McCalmont, S. L. James, A. Porcheddu, F. Delogu, D. E. Crawford, E. Colacino and S. Spatari, *ACS Sust. Chem. Eng.*, 2022.